eng

MDPI

Article

Engineered Armor Unit for Rubble Mound Breakwaters: Stability and Structural Response Evaluation

Mohammed Zuhear Al-Mulali [1], Sally Selan Hussein [2], Haneen Fadhil [2], Zahraa Hazim Obaid [3], Abdullah Kadhim [4], Merzah Kareem Imran [2], Lina Fahem Wannas [5], Zahraa Eisa [6], Tameem Mohammed Hashim [2], Mohammed Salah Nasr [7] and Ali Shubbar [8,*]

1 Department of Civil Engineering, College of Engineering, University of Baghdad, Baghdad 10071, Iraq; mohammed.almulali@coeng.uobaghdad.edu.iq
2 Building and Construction Techniques Engineering Department, College of Engineering and Engineering Techniques, Al-Mustaqbal University, Babylon 51001, Iraq
3 Electrical Engineering Techniques Department, College of Engineering and Engineering Techniques, Al-Mustaqbal University, Babylon 51001, Iraq
4 Department of Civil Engineering, College of Engineering, Al-Qasim Green University, Babylon 51013, Iraq
5 Department of Civil Engineering, College of Engineering, Al-Turath University, Baghdad 10017, Iraq
6 Medical Instrumentation Technique Engineering Department, College of Engineering and Engineering Techniques, Al-Mustaqbal University, Babil 51001, Iraq
7 College of Engineering, University of Babylon, Babylon 51001, Iraq; eng511.mohammed.nasr@uobabylon.edu.iq
8 School of Civil Engineering and Built Environment, Liverpool John Moores University, Liverpool L3 5UX, UK
* Correspondence: a.a.shubbar@ljmu.ac.uk

Abstract

Designing armor units that can withstand harsh marine environments while remaining cost-effective is a central challenge in modern breakwater engineering. This study introduces a newly designed artificial armor unit and evaluates its performance in comparison with established alternatives such as the accropode, core-loc, and conventional rock armor. The findings reveal that the new unit achieves a lower packing density, reducing the number of units required and thereby improving overall cost-effectiveness. Armor layers formed from the newly designed unit exhibited higher porosity than accropode but lower than core-loc, effectively avoiding the slender geometries that compromise durability. Structural analysis using STAAD.Pro confirmed that the new unit developed lower tensile stresses, with reductions of 15% compared to accropode and 35% compared to core-loc under flexure, torsion, and combined loading, demonstrating superior integrity. Hydraulic stability tests showed that the randomly placed newly designed units resisted failure at a stability number (N_s) of 1.4, lowering run-up by 50% and overtopping by 59%, while the uniformly placed newly designed units reached 1.5 without failure, with run-up and overtopping reductions of 30% and 37%, respectively. Collectively, these outcomes highlight the clear hydraulic and structural advantages of the new design over conventional systems, establishing it as a stronger and more resilient solution for breakwater protection.

Keywords: artificial armor unit; hydraulic stability; structural integrity; packing density; overtopping; economic efficiency

Academic Editor: Wanli Yang

Received: 30 November 2025
Revised: 4 January 2026
Accepted: 14 January 2026
Published: 1 February 2026

1. Introduction

1.1. Research Background

Throughout history, great civilizations like the Greeks, Romans, Mesopotamians, and Egyptians thrived near the sea, as coastal locations symbolized wealth, prosperity, and

strength [1]. The sea provided a sustainable food source, facilitated trade, which advanced technology and weaponry, enabled cultural exchange, and served as a natural defense against invasions [2]. Despite these advantages, coastal locations also face challenges from storms and high waves, which can lead to erosion and flooding [3]. To minimize human and property loss, various measures were implemented to protect coastal areas and waterways [3].

Previous studies classify coastal defense methods into two types: soft and hard. The soft approach relies on natural sediment to reduce wave impact. Beach nourishment, a common soft coastal defense method, restores eroded beaches by adding sand. Although it avoids physical barriers, it has drawbacks such as reduced water clarity, short refill lifespan, and inconsistent performance [4]. On the other hand, the hard approach to coastal defense uses physical barriers to reduce wave impact and prevent erosion. As a traditional method, it remains widely used due to extensive research, perceived security, and the need to safeguard high-value coastal areas [4].

Coastal defense structures are classified into onshore, shore-detached, and offshore types. Onshore structures, like sea walls and revetments, are built parallel to the coast using stone or concrete to prevent erosion [5]. They are preferred for protecting valuable hinterland, even at the cost of beach erosion [5]. Shore-detached structures, like groins and jetties, are built perpendicular to the coast. Groins are smaller and placed in groups, while larger jetties extend further offshore [6]. They control sediment movement and protect harbors but may cause downdrift erosion [6].

Offshore structures, or breakwaters, are built away from the coast to reduce wave impact. The main types are rubble mound and caisson breakwaters [7]. Rubble mound breakwaters, made of quarry rock and concrete, help reduce wave action and promote beach formation by intercepting sediment movement [8].

While coastal locations offer many benefits, they also face erosion and flooding, exacerbated by global warming. Rising sea levels and stronger storms heighten flood risks, while increasing wind speeds intensify waves, threatening beaches and coastal areas [9]. Additionally, many coastal countries are expanding into the sea, but those near tectonic plate boundaries face earthquake and tsunami risks, leading to severe property damage and loss of life [10]. Engineering challenges also arise, as large rock armor units (10–15 tons) are scarce and face structural and economic limitations [11]. In addition, real-life events have underscored the vulnerability of traditional RMBWs, for example, armor layer failure when subjected to waves caused by severe storms such as Typhoon Mangkhut in 2018 [12], and the Black Sea storm in the same year which led to severe structural damage in which core erosion and crown wall collapse occurred [13].

These examples highlight the critical importance of the stability number in armor design. Although this study is a preliminary hydraulic assessment, it aims to evaluate a new armor unit that has the ability to mitigate these issues facing the infrastructure through providing enhanced stability and overtopping risk reduction [14,15].

Such challenges emphasize the need for stronger, more stable, and cost-effective alternatives with higher structural integrity. The newly designed artificial armor unit will offer better hydraulic performance, greater stability, reduced overtopping and run-up, improved porosity, and better cost-effectiveness compared to rock armor units and other artificial armor units.

1.2. Literature Review

Many previous studies have examined the design of new concrete units for offshore breakwaters, focusing on durability, hydrodynamic performance, and environmental compatibility, while also addressing the challenges and benefits of sustainable coastal protection

solutions. Additionally, research on rubble mound breakwaters (RMBWs) has categorized key aspects such as stability, overtopping, and run-up, analyzing the effects of rock and concrete armoring. This discussion begins with a detailed description of a typical rubble mound breakwater and its structural requirements. An RMBWs is a sloped structure made of layered rock, with a core of quarry-run rock, intermediate layers, and outer armor units to dissipate wave energy, as shown in Figure 1.

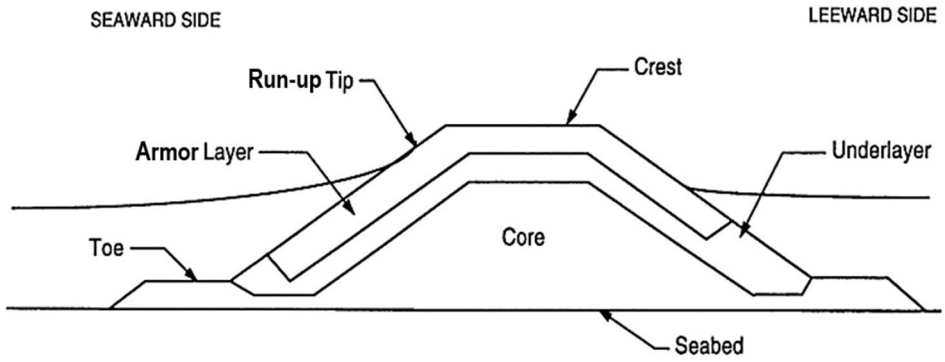

Figure 1. Cross-section of a typical (RMBWs).

Hudson's early work on RMBWs instituted a basic empirical equation for sizing armor units depending on an extensive physical modeling program using regular waves [16]. The created formula directly relates wave height, density of the used material, slope angle, and the stability coefficient. However, Hudson's formula was limited to regular waves, and it cannot be adopted when surf zone processes, wave breaking, and storm duration are vital information to take into consideration. Van der Meer [17] conducted systematic experiments under random waves in which he expanded the understanding of armor unit stability along with damage parameters that take into consideration wave period, storm duration, permeability, and wave breaking mode.

Sayar SD et al. [18] examined the hydraulic performance of eco-friendly breakwaters, assessing wave effects and habitat benefits. They compared traditional and ecological designs using models, highlighting their potential for both coastal protection and biodiversity.

Safa E et al. [19] evaluated a new nature-based armor unit for rubble mound breakwaters, finding that it reduced wave impact and improved energy dissipation, offering a sustainable solution to enhance breakwater stability and durability. Park YH et al. [20] developed a new concrete armor unit to withstand high waves and enhance coastal protection. The results indicated that the unit exhibited improved hydraulic stability, wave energy dissipation, and structural integrity, making it a durable and effective solution for high-wave environments.

Leone E et al. [21] evaluated the overtopping performance of a rubble mound breakwater with innovative armor units using physical and numerical modeling. The results indicated that the new armor units significantly reduced overtopping, improving the breakwater's hydraulic performance and enhancing coastal protection. In addition, Mousavi SH et al. [22] conducted an experimental analysis of breakwater stability using Antifer concrete blocks. The findings revealed that these blocks significantly improved structural stability and wave resistance, making them a dependable solution for breakwater reinforcement.

Suwondo R et al. [14] demonstrated that improving armor stability coefficients can enhance the hydraulic, economic, and environmental performance of rubble mound breakwaters within conventional design frameworks. Building on this approach, the present study advances the field by shifting the focus from parameter optimization to geometry-driven armor unit design, showing that enhanced interlocking and structural compactness

can fundamentally improve stability. This progression supports the development of future breakwater solutions that are more resilient, scalable, and sustainable.

Khodadoust H [23] applied a multi-criteria framework to evaluate armored breakwater alternatives by balancing hydraulic, economic, and environmental factors, while the present study advances breakwater performance at the armor-unit level through geometry-driven design that enhances inherent stability and resilience.

1.3. Research Novelty

The novelty of this study lies in the development of a new concrete armor unit specifically designed for offshore breakwaters, aimed at surpassing the performance of traditional rock armor. Unlike existing studies, the proposed unit is comprehensively evaluated against widely used artificial armor systems, considering key factors such as porosity, packing density, hydraulic stability, and structural integrity, while also addressing cost-effectiveness. This integrated approach highlights the unit's potential advantages and establishes its contribution as a more efficient and durable solution for coastal protection.

1.4. Research Main Objectives

This study aims to design a new, cost-effective armor unit with superior hydraulic performance through a three-step approach: concept development, hydraulic testing in two-dimensional flumes, and comparative evaluation with existing armor units. The key objectives are to achieve better interlocking than rock armor, enhance hydraulic stability while reducing run-up and overtopping, and ensure structural integrity with higher porosity. In addition, the study seeks to realize a lower packing density than conventional artificial units, thereby improving both efficiency and resilience of the new design.

2. Methodology

RMBWs simply consist of several components that provide both hydraulic performance and structural stability. The core, commonly constructed from quarry-run rock or geotextile tubes filled with sand, provides necessary permeability to disperse wave energy and should be designed to avoid material segregation [24]. On the seaward side, toe protection provides stability for the armor layer. The underlayers offer both filter and structural support, in which they are commonly arranged in two or more stone-thick layers of rocks that are sized beneath the primary armor [25]. The slope angle further influences the RMBWs' structural stability, where slopes on the seaward side range from 1:1.5 for rock armor units to 1:1.33 for interlocking concrete units. Width and elevation of the crest are dependent on both overtopping limits and construction requirements; at least three rows of armor units are usually incorporated.

2.1. Armor Layer

The armor layer, made of rock or designed units, resists waves with a set slope and thickness. Units can be systematically or randomly placed, with stability critical to the structure's success [26]. The types of armor layers are briefed below:

1. Rock armor units

Rock is commonly used for armor units in rubble mound breakwaters, but sourcing large rocks (10–15 tons) can be challenging for local quarries, with transportation costs adding further economic difficulties. The most common types of rock armor are as follows [27]:

- Random-shaped rocks
- Polygonal armor units
- Core-layer rocks

- Artificial rock units
- Riprap

Figure 2 demonstrates the different types of rock armor.

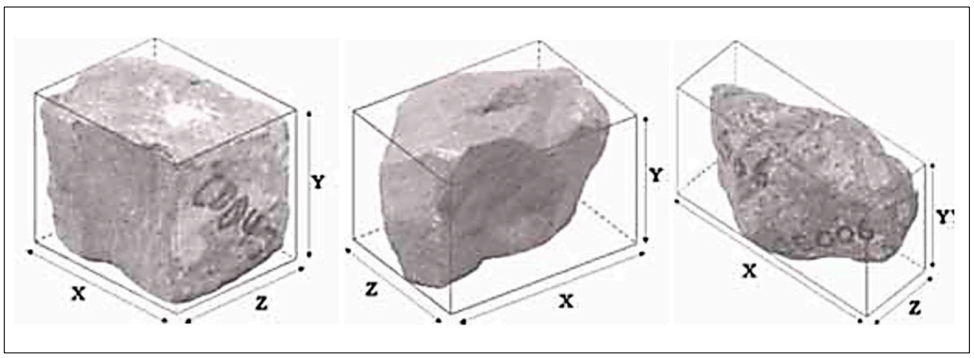

Figure 2. Different types of rock armor.

2. Concrete armor units

When choosing stone armor units for a cover layer, if the desired size is unavailable or not cost-effective, alternatives should be evaluated. Concrete armor units serve as a practical replacement, providing a higher stability coefficient. This allows them to be placed on steeper structure slopes while also reducing the required weight of the armor units. The most common types of concrete armor are listed below [28]:

- Tetrapod
- Dolos
- Accropode
- Core-loc
- Cube
- Xbloc
- A-jacks
- Riprap (modified concrete variants)

Figure 3 demonstrates the different types of concrete armor.

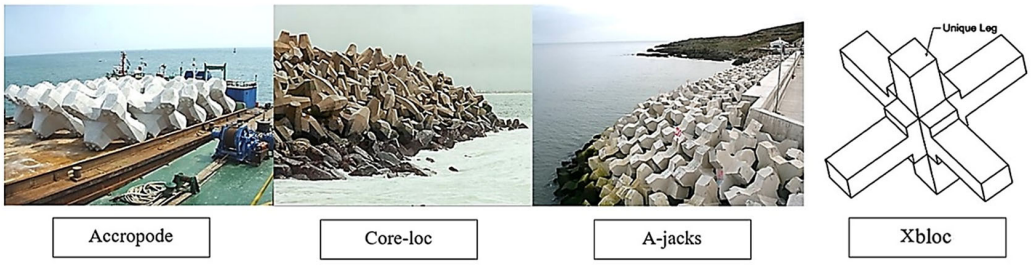

Figure 3. Different types of concrete armor.

2.2. Design Adoption

This study aims to develop an interlocking concrete armor unit that can be arranged either randomly or uniformly in a single layer. The redesigned unit should also incorporate the following:

- A hydraulic stability similar to that of accropode and core-loc;
- A robust shape that gives it higher structural integrity;
- A concrete demand less than that of accropode and core-loc.

Design Concept

As shown in Figure 4, the unit exhibits a simple, robust geometry that is easy to fabricate and contains no slender components. It is suitable for single-layer application, with a design that provides strong interlocking capability and allows placement either randomly or uniformly on a slope.

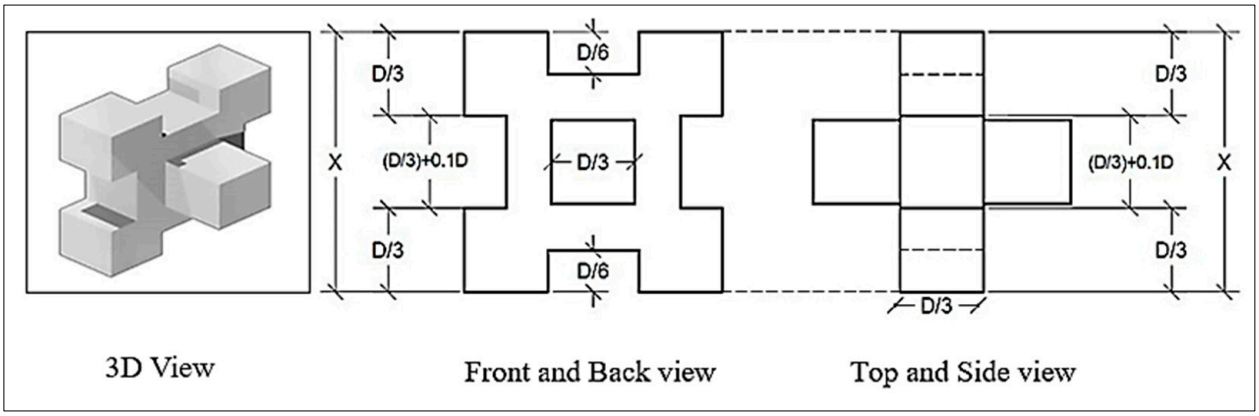

Figure 4. Proposed armor unit and its proposed geometry.

To make a comparison with more established single-layer armor units such as the accropode and Xbloc, the proposed interlocking concrete unit provides several advantages. The orthogonal prismatic geometry enables simpler and cost-effective mold fabrication, providing cost reduction while enhancing dimensional consistency and quality control during casting. The thick, compact arms ensure great structural robustness and lower risk of damage when handling, transporting, and placing, which is an issue encountered with more slender proprietary units. The proposed armor unit provides reliable mechanical interlocking and stable packing when used on typical design slopes and at the same time requires less specialized operator training and placement procedures.

2.3. Geometric Configuration of the Proposed Armor Unit

The newly designed concrete armor unit consists of a daisy-shaped central core with two symmetrically attached cube-like arms, resulting in a geometry with two primary faces as in Figure 4. The unit is designed to promote interlocking between adjacent elements, enhancing hydraulic stability while maintaining ease of placement.

The basic design formulae and concrete armor unit parameters are listed in the rock manual by the Construction Industry Research and Information Association CIRIA C683 (2007) [29], as shown in Table 1 below.

For the recently introduced concrete armor unit, the equations provided in Table 1 are applied to calculate the layer coefficients, porosity (the percentage of voids inside the armor layer in relation to the total volume), and packing density (describes how tightly the armor units are arranged within the armor layer). These calculated values are then compared with the parameters of other artificial armor units, which are imbedded in the rock manual CIRIA C683 (2007) [29], and presented in Table 2 below.

Table 1. Geometric design parameters for random armor units—CIRIA C683 (2007) [29].

Parameter	Equation	Equation No.
Armor unit volume, nominal diameter, and characteristic length	$V = (M/\rho_c) = D_n^3 = k_s D^3$	(1)
Center-to-center distance between armor units	$\Delta_x = X_c\ D = X\ D_n$; $X = X_c/k_s^{1/3}$ $\Delta_y = Y_c\ D = Y\ D_n$; $Y = Y_c/k_s^{1/3}$	(2)
Area covered by one armor unit	$A_a = \Delta_x\ \Delta_y = X_c\ Y_c\ D^2 = X\ Y\ D_n^2 = n/N$	(3)
Armor layer thickness	$t_a = n\ k_t\ D_n = n\ k_c D$; $k_c = k_t\ k_s^{1/3}$	(4)
Armor layer porosity	$n_v = 1 - nV/(A\ t_a) = 1 - k_s^{2/3}/(X_c\ Y_c k_t)$ $= 1 - 1/(XYk_t)$	(5)
Packing density coefficients	$\Phi = nk_t\ (1 - n_v)$	(6)
Number of units per unit area	$N = \Phi/D_n^2 = \Phi/V^{2/3}$	(7)
Concrete volume	$V_c = NV = t_a\ (1 - n_v)$	(8)

A: Total surface area (m^2) of armor layer panel parallel to slope; D: Area covered by one armor unit (m^2), equal to: nA/N_a; D_n: Nominal armor unit diameter (m), the equivalent cube size; k_c: Modified layer coefficient (-); k_s: Shape coefficient (-); k_t: Layer coefficients (-); N: Number of armor units per unit area ($1/m^2$); N_a: Total number of armor units placed on surface area (-); n: Number of layers; n_v: Armor layer porosity (-); t_a: Armor layer thickness (m); V: Armor unit volume (m^3); V_c: Concrete volume per unit area (m^3/m^2); M: Armor unit mass; X, X_c: Dimensionless horizontal distance (-); Y, Y_c; Dimensionless upslope distance (-); Δ_x, Δ_y: Horizontal and upslope center-to-center distance between units (m); Φ: Packing density coefficients (-); ρ_c: Density of concrete (kg/m^3).

Table 2. Parameters for several armor units—CIRIA C683 (2007) [29].

Armor Unit Type	Size (m^3)	Layer Coefficients	Shape Coefficient	Distance Between Units		Porosity	Packing Density Coefficient	Modified Layer Coefficient	Recommended Slope
				Horizontal	Slope-Parallel				
		k_t (-)	k_s (-)	Δ_x/D_n (-)	Δ_y/D (-)	n_v (-)	Φ (-)	k_c	Cot α (-)
Rock (quarried stone, angular/boulders)	-	1.0	0.8	1.0	1.0	0.4	0.56	1.0	1 to 1.5 1 to 2
Cube (two layers) [1]	-	1.10	1.0	1.70	0.85	0.47	1.17	1.10	-
Tetrapod Dolos (r = 0.32)	-	1.02 0.94	0.280 0.16	1.98 2.19	0.99 1.10	0.5 0.56	1.02 0.83	0.667 0.51	4/3 to 1.5 2 to 3
Accropode	<5	1.29	0.341	1.77	0.86	0.491	0.656	0.9021	4/3 to 1.5
	5–12			1.82	0.91	0.531	0.605		
	>12			1.86	0.93	0.552	0.578		
Core-loc	<5	1.516	0.2236	1.83	0.91	0.605	0.598	0.9201	4/3 to 1.5
	5–8.5			1.85	0.92	0.613	0.587		
	8.5–12			1.85	0.93	0.613	0.580		
	>12			1.87	0.92	0.624	0.569		
Xbloc	<5	1.40	0.333	1.87	0.92	0.587	0.578	0.97	4/3 to 1.5
	5–12			1.92	0.94	0.603	0.552		
	>12			1.96	0.97	0.623	0.528		
Cube (one layer)	High [2]	1.0	1.0	1.33	1.00	0.25	0.75	1.0	-
	Low [2]			1.70	0.85	0.31	0.69		

Notes: [1]. r = waist-to-height ratio (waist diameter of central section and total height of unit); [2]. Packing density.

2.4. Structural Integrity

The structural integrity of the newly designed armor unit is presented in this section. Structural integrity refers to the unit's ability to withstand stresses caused by wave energy dissipation and handling. The STAAD.Pro software (STAAD.Pro V8i) is used to analyze and determine the level of stress the new design can endure. Figure 5 shows the loading and fixing schemes used in this study. To determine the stress levels for the newly designed

unit, a unit with a volume of 8.65 m^3 was selected. The unit is made of concrete, chosen from the material options available in the STAAD.Pro software. The selected concrete has a density of 23.5616 kN/m^3, a Young's modulus (E) of 21,718,456 kN/m^2, and a Poisson's ratio (ν) of 0.17.

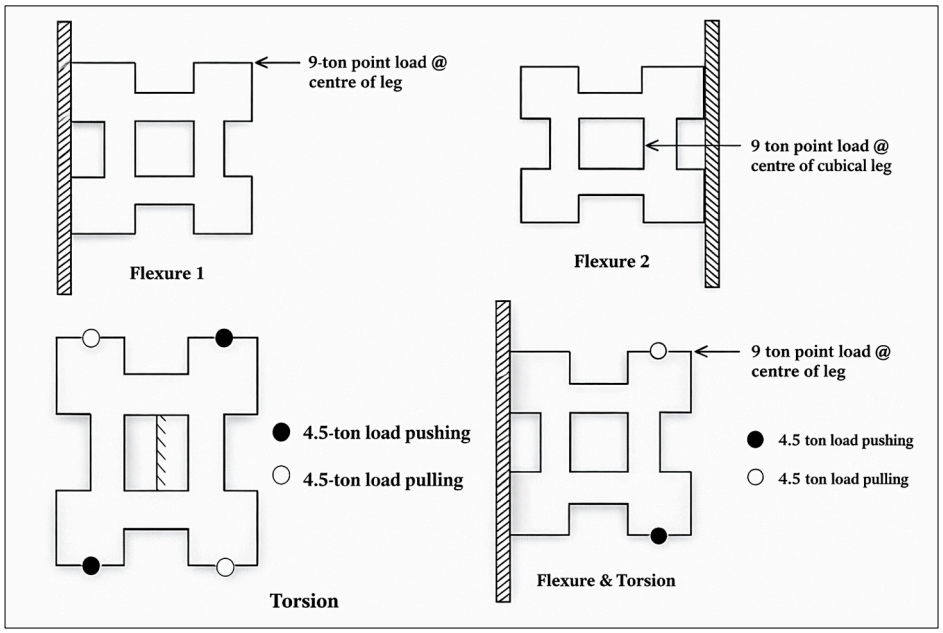

Figure 5. Loading schemes for the newly designed armor unit.

2.5. Possible Placement Arrangements

This section presents various possible placement configurations for the new armor unit. These configurations are tested using concrete models with a volume of 72 cm^3 and a height of 6 cm. The models are positioned within a specific area measuring 21.5 cm × 34.0 cm.

2.5.1. First Placement

This placement configuration allows 20 units to be positioned within the specified area. The units are oriented at a 45-degree angle relative to the *x*-axis of the area. The height of this layer is 4.5 cm. Figure 6a illustrates this placement configuration.

2.5.2. Second Placement

This placement configuration allows 21 units to be positioned within the specified area. The units are stacked parallel to the area's axes. The height of this layer is approximately 4.5 cm. Figure 6b illustrates this placement configuration.

2.5.3. Third Placement

In this method, the units are stacked randomly. The maximum height of this layer corresponds to the height of an individual unit, which is 6 cm. This placement method accommodates 22 units within the specified area. Figure 6c illustrates this placement configuration.

2.5.4. Fourth Placement

This placement configuration allows 24 units to be stacked within the specified area. The thickness of this layer is 4.5 cm. This placement configuration is illustrated in Figure 6d.

The geometry of the proposed newly designed armor unit provides four feasible placement schemes due to its symmetric arm configuration and balanced mass distribution. The uniform and patterned arrangements shown in Figure 6 are the only patterns feasible and could be recommended for safe and efficient on-site stocking. They promote stability

and space efficiency because of the orderly nature in which they allow the armor units to be stacked in stable, nested layers, leading to the conservation of valuable casting yard space and ensuring worker safety. In contrast to these patterns, the randomly placed unit pattern, as shown in Figure 6c, is strictly a placement scheme used on breakwater slopes and is unsuitable for storage due to its unpredictable, dangerous, and unstable stacking arrangement.

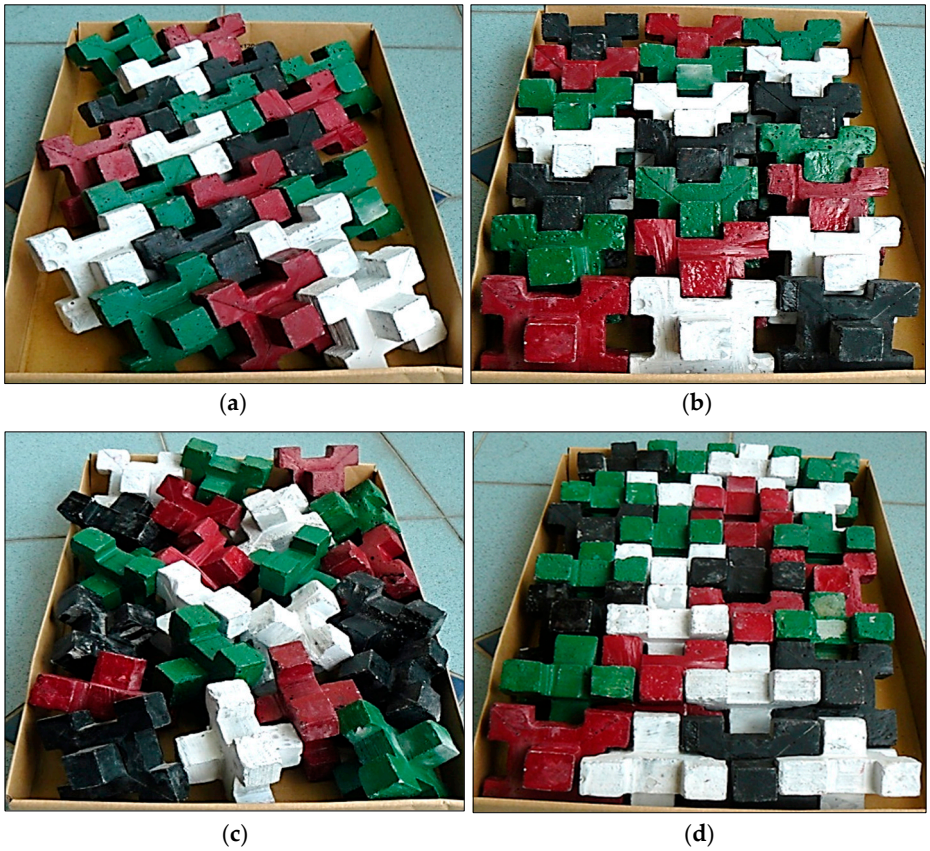

Figure 6. Possible placement configurations. (**a**) First placement, (**b**) second placement, (**c**) third placement, and (**d**) fourth placement.

Therefore, one of the three uniform patterns will be selected (the arrangement shown in Figure 6b) to be tested along with the random placement scheme for their on-slope performance. These tests will be thoroughly described in the coming sections.

2.6. Laboratory Work

The upcoming sections will outline the experimental set-up for testing a newly designed concrete armor unit's hydraulic response and stability, compared against a rock armor layer. The study examined overtopping and run-up for the new unit, but transmission and reflection were not tested due to equipment limitations. The testing process is split into three phases: unit fabrication, cross-section design, and the testing phase itself.

2.6.1. Phase One (Unit Fabrication Phase)

A series of trial-and-error experiments were conducted to fabricate a concrete unit model. This process involved designing a durable mold and selecting a suitable mortar mix that could be easily poured and remain intact after drying.

Mold Design Process

The mold design process involved multiple trials. Initially, a two-piece wooden mold was used but failed due to its rough interior causing mortar adhesion. A second attempt with a two-piece steel mold also failed due to air suction between the halves. Ultimately, a multi-component plywood mold was chosen for its cost-effectiveness and ability to accelerate fabrication. Figure 7 illustrates the mold design and its actual dimensions.

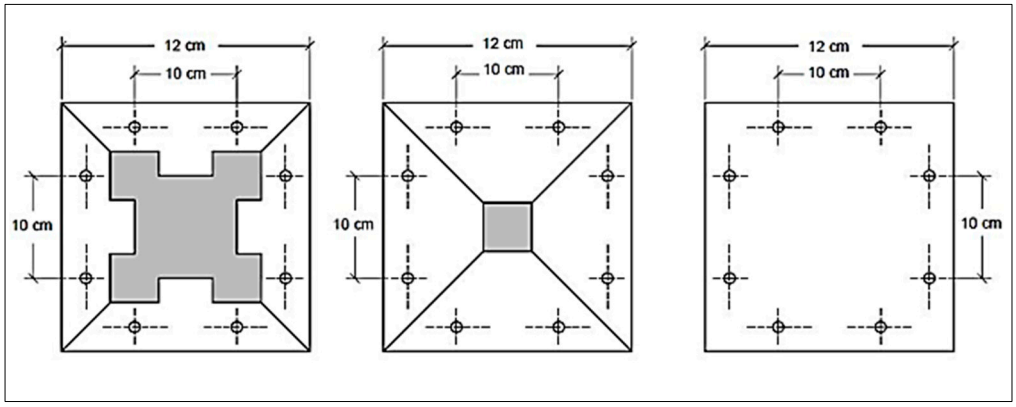

Figure 7. Mold dimensions.

Figure 8 illustrates the mold's four-layer design with actual dimensions. The first and third layers shape the unit's attached cubes, the second layer forms its faces, and the fourth layer serves as the base. Each layer, except for the fourth, consists of four parts to achieve the desired shape.

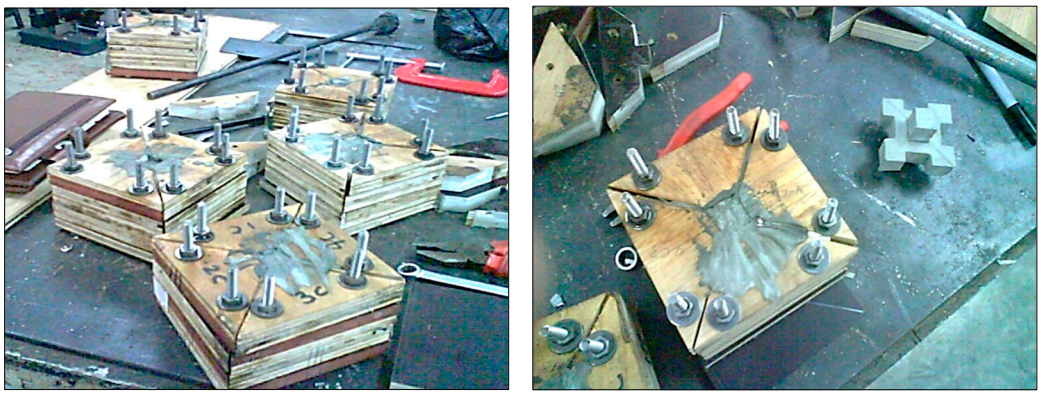

(**a**) (**b**)

Figure 8. Fabrication procedure. (**a**) Complete molds and (**b**) mold with a casted unit.

Mortar Mix

The selected mortar needed to be easy to pour, simple to prepare, and durable when dry. Initial mixes of sand, cement, and water were difficult to pour and caused weak points in the model.

A cement slurry (cement and water) was chosen instead, ensuring better flow, minimal leakage, and appropriate hardening time. The final mix had a 2:1 cement-to-water ratio with a density of 1700 kg/m^3.

Fabrication Procedure

The molds were cleaned and oiled before casting. Sufficient mortar was prepared and gradually poured into the molds with vibration to prevent air bubbles. The casted molds were left to dry for 24 h before the models were removed and wrapped in plastic for

curing. This process produced 130 units, each with an average weight of 122 g, a density of 1700 kg/m^3, and a volume of 72 cm^3. Figure 8a,b show the fabrication procedure

2.6.2. Phase Two (Structure Cross-Section Design)

This study focuses on testing a new armor unit for its hydraulic stability and response by designing a theoretical rubble mound breakwater. The breakwater is emergent, has two layers and a core, and lacks toe support and a concrete crown. For comparison, rock armor units, chosen for their abundance and ease of use, are paired with the new units, both having an average individual weight of 122 g. The underlayer stones weigh 22 g (1/5 to 1/10 of the armor layer), and the core, made of crushed stone under 10 mm, weighs 1.1 g (1/20 of the underlayer). The armor layer thickness is set at 6 cm, matching the artificial unit's height. A slope of 1:1.5 is selected as it suits both rock and artificial units. The new armor units are tested in two configurations, random and arranged placements, to evaluate the preliminary hydraulic stability. A narrow 2D wave flume was chosen to make a comparison between the newly designed armor unit's hydraulic stability and conventional rock armor under controlled flow conditions. The limited width allows for uniform loading across both armor types and limits unwanted lateral dispersion. Typically, rock armor units rely on mass and surface roughness for hydraulic stability, while the newly designed armor unit depends on interlocking, geometry, and orientation. The narrow flume helps to expose these behavioral differences by creating consistent turbulence levels and repeatable shear stresses on each set-up. This will make it possible to obtain the threshold at which each armor type begins rocking, sliding, or displacing, enabling a fair and efficient basis for evaluating if the newly designed armor unit offers improved hydraulic performance before advancing to broader physical testing. In addition, the narrow flume provides a controlled environment to study the performance of the newly designed armor unit when subjected to regular waves, including how the units interact and interlock among themselves. Figures 9 and 10 illustrate the random and arranged placements of the units, respectively, from a plan view. Figures 11 and 12 depict both the rock armor layer and the armor layer composed of randomly placed, newly designed armor units.

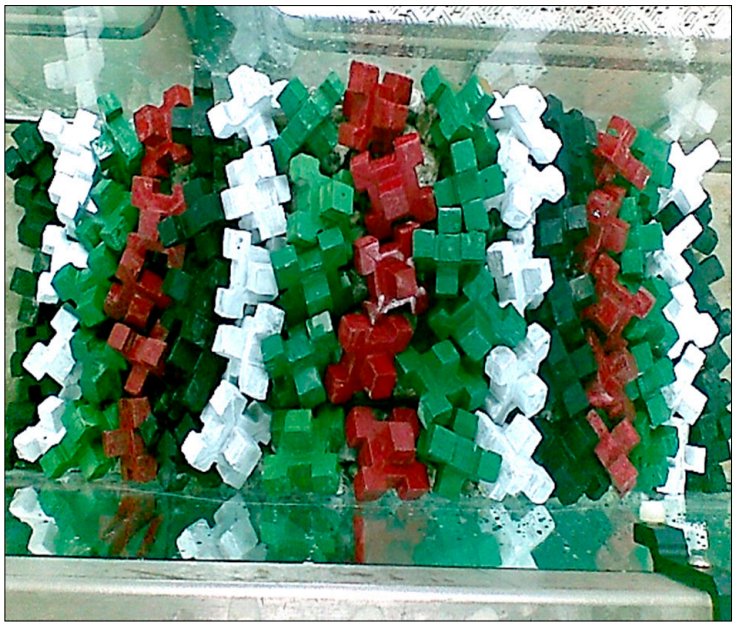

Figure 9. Top view of randomly placed, newly designed units.

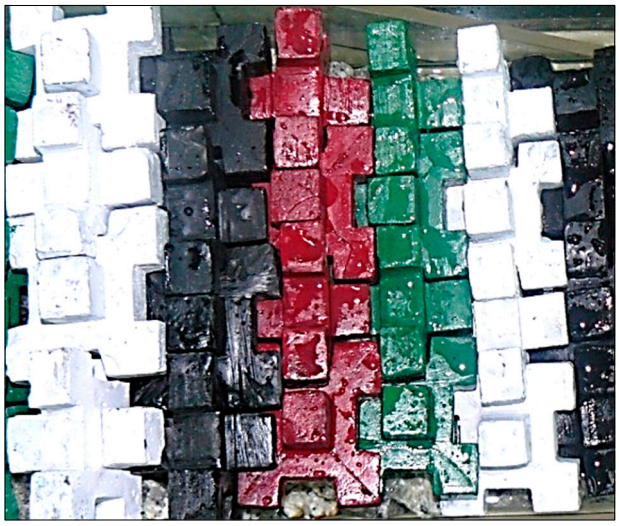

Figure 10. Arranged placement of the newly designed armor unit.

Figure 11. Rock armor layer.

Figure 12. Front view of randomly placed, newly designed armor units.

Figures 13 and 14 illustrate the cross-sections of the theoretical structure for the rock armor layer and the layer of uniformly placed newly designed units, respectively.

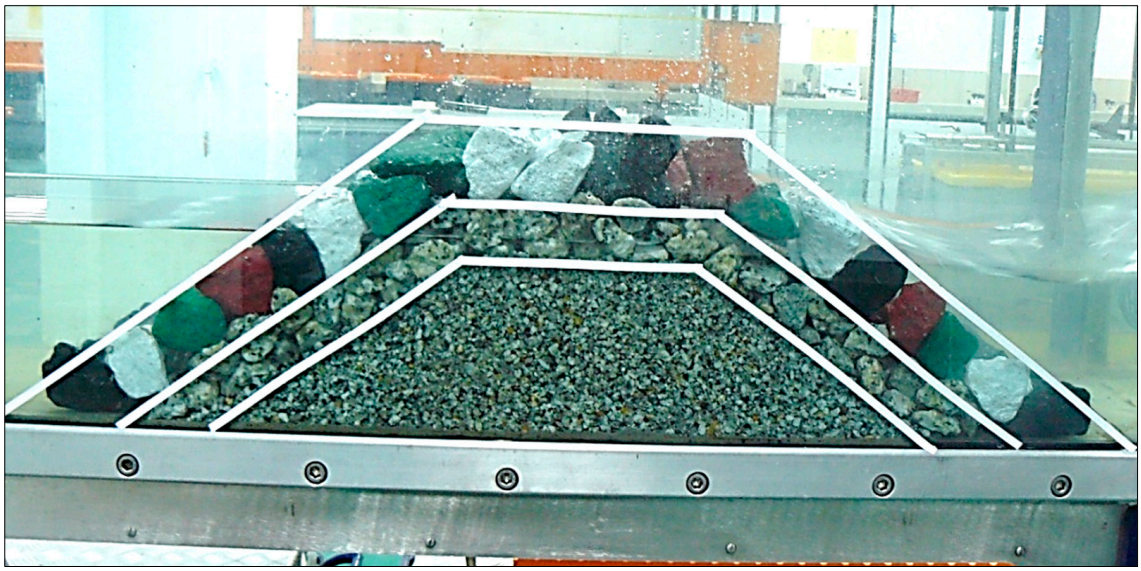

Figure 13. Cross-section of the theoretical structure with rock armor layer.

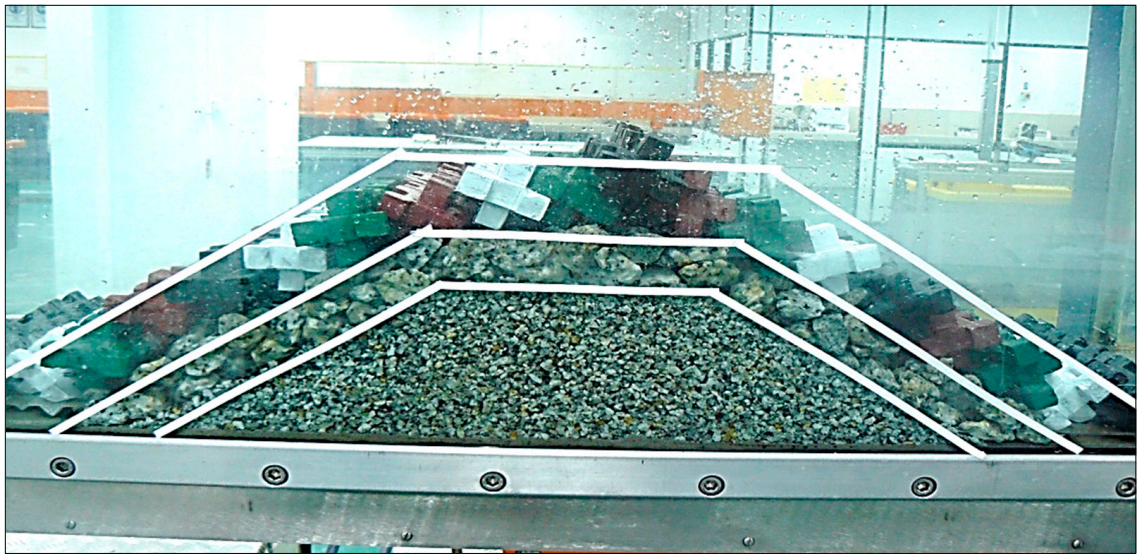

Figure 14. Cross-section of the theoretical structure with a layer of uniformly placed newly designed units (first orientation).

2.6.3. Phase Three (Experimental Set-Up)

Two-dimensional tests were conducted to evaluate the hydraulic stability and response of the new armor unit. These tests utilized an Armfield S6 MKII (Armfield Ltd., Ringwood, UK) tilting flume following the guidance of CIRIA C683 [29], which has a length of 10 m, a height of 45 cm, and a width of 30 cm. This flume can generate small, regular surface waves. Waves were produced using a motor-powered paddle (Armfield Ltd., Ringwood, UK) at the upstream end. The paddle vacillates horizontally, hence producing periodic disturbances down the flume, generating regular waves. Figure 15 shows the flume used in the tests.

Figure 15. Hydraulic flume with the wave generator.

A rod connected the motor's flywheel to the paddle. Adjusting the rod's position on the flywheel produced a range of wave heights. The motor operated at a constant speed of 100 revolutions per minute, and a consistent mean wave period of 0.63 s was maintained throughout the tests. Manual point gauges were used to determine wave heights. It is worth mentioning that the Reynold's number is approximately 0.0003. The obtained value agrees with the standard criteria for neglecting viscous scale effects when testing RMBWs.

Although the flume is considered small for rigorous hydraulic stability testing, the goal of this research is the comparison of hydraulic behavior between the newly designed armor unit and rock armor under controlled, repeatable flow-generated waves. Early comparison of rocking, sliding, or displacement can be performed effectively in small flumes such the one used in this study. At this stage, performance comparisons of the tested armor units outweigh the need for reliable wave modeling.

2.6.4. Hydraulic Stability

The study used two-dimensional experiments to evaluate the hydraulic stability of a new armor unit. The cross-section, adhering to phase two guidelines, was set at a height of 25 cm (based on the flume's waterway) to avoid water spillage, spanned the flume's 30 cm width, and was placed 5 m from the wave generator where waves broke. A 12 cm water depth was chosen to ensure consistent waves, with the height being the only pre-set design factor. The stability number (Ns = H/ΔDn) was correlated with the surf similarity factor (ξ) to determine the stability numbers for both rock and the new armor unit in both placements. The Hudson formula was employed to obtain the stability number and the surf similarity number was obtained through the following formula:

$$\xi = \frac{\tan \alpha}{\sqrt{H_0 / L_0}}$$

where α is the slope angle, H_0 is the incident wave height, and L_0 is the deep-water wavelength, which was determined from the linear wave theory relationship:

$$L_0 = \frac{gT^2}{2\pi}$$

with T representing the wave period and g the gravitational acceleration.

2.6.5. Run-Up

Run-up was tested for both the rock armor layer and the armor layer composed of the new armor unit. The same cross-section used in the hydraulic stability test was applied here. Additionally, the same orientation as in the first experiment was maintained. Run-up was measured by determining the distance the wave climbed on the structure's slope above the water level. Figure 16 shows the run-up (R) for the rock armor layer.

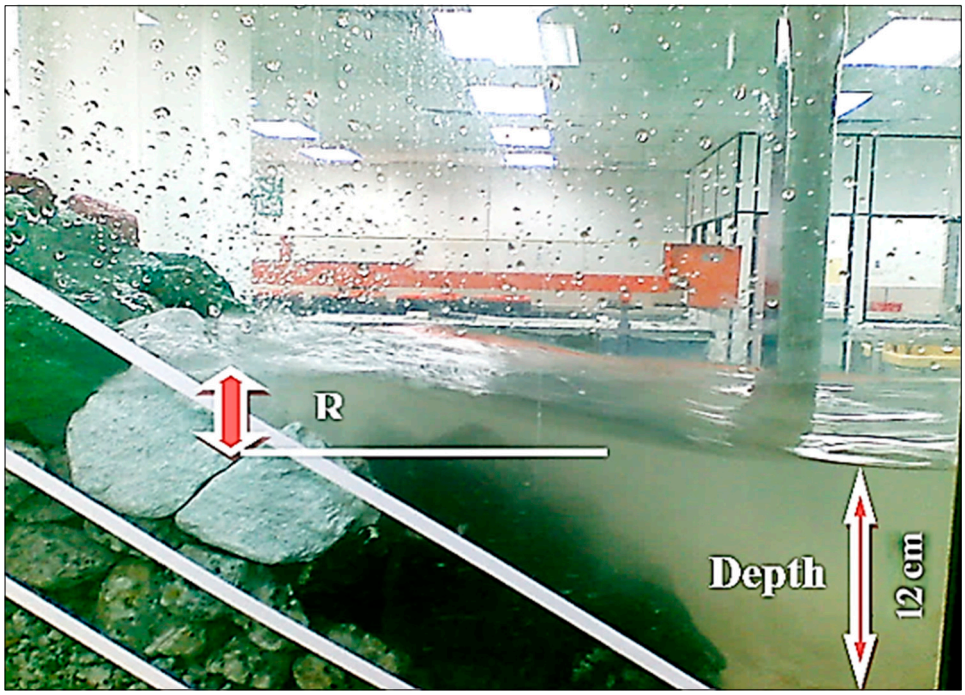

Figure 16. Run-up testing using the first orientation.

2.6.6. Overtopping

A different testing scheme was used for overtopping. To measure the quantity of overtopping, a specific structure was constructed. The fabricated structure was made of Perspex and had the same slope and height as the cross-section used in previous tests, but with a narrower width, holding only half of the original cross-section. It also contained a water basin with the same height as the structure (25 cm), a width of 20 cm, and a length of 10 cm.

The purpose of this test was to allow overtopping to occur over the slope. This was achieved by subjecting the cross-section to waves of constant height and period while maintaining a high water depth at the toe of the structure (up to 20 cm). As a result, the freeboard (the distance between the crest level and the water level) was 5 cm. The test procedure involved measuring the amount of water collected in the basin for each armor layer. Figure 17 shows the top view of the basin used for this test, while Figure 18 illustrates how the test was conducted.

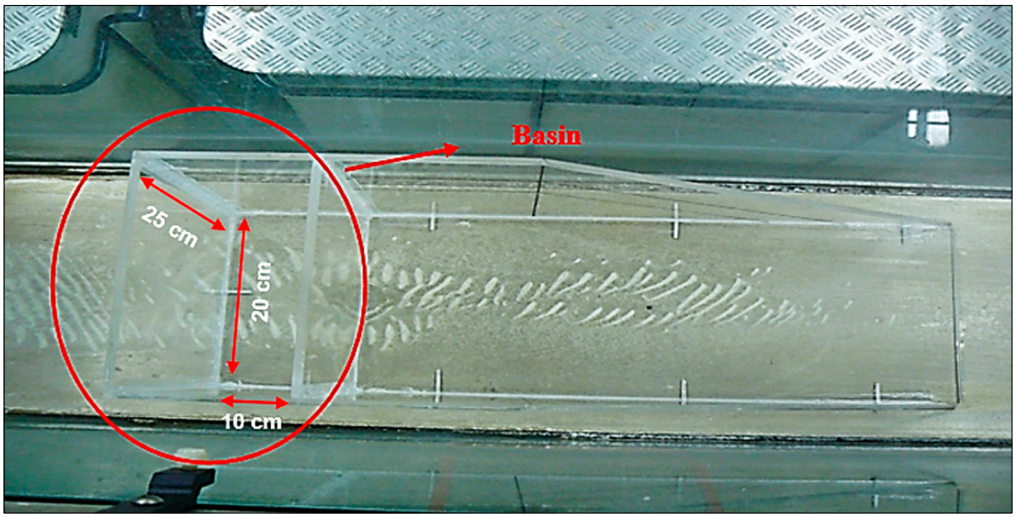

Figure 17. The fabricated structure for testing the overtopping.

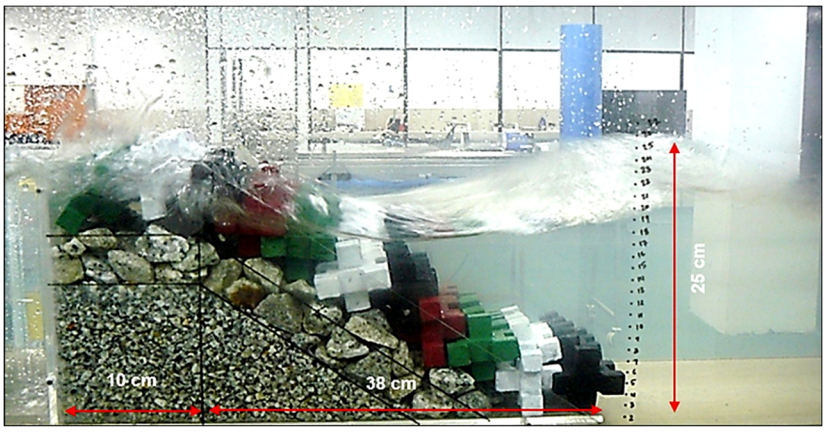

Figure 18. Overtopping testing using the second orientation.

3. Results and Discussion

3.1. Layer Coefficients and Parameters

The rock manual provides design parameters and formulas to determine armor layer characteristics, including layer coefficients (Ks, Kt, Kc), porosity, and packing density. Table 3 presents results for the newly designed armor unit on a 1:1.5 slope, compared with other units in Table 2. Table 3 details layer coefficients, porosity, and packing density for randomly placed units. Measurements included both horizontal and upslope distances. The stability coefficient (Ks) was calculated from the unit volume and characteristic length, while (Kt) was derived from the layer thickness and scale ratio. The full-scale units tested were 4.5 m^3, 8 m^3, and 13 m^3 in volume.

Table 3. Parameters for the newly designed concrete armor unit.

Size of Unit (m^3)	Layer Coefficient K_t	Shape Coefficient K_s	Porosity n_v	Packing Density Φ	Modified Layer Coefficient K_c
<5	1.4	0.32	0.588	0.577	0.96
5–12			0.60	0.560	
>12			0.601	0.559	

These results were compared with the porosity and packing density of the accropode and core-loc units in accordance with CIRIA C683 (2007) [29], as shown in Figure 19.

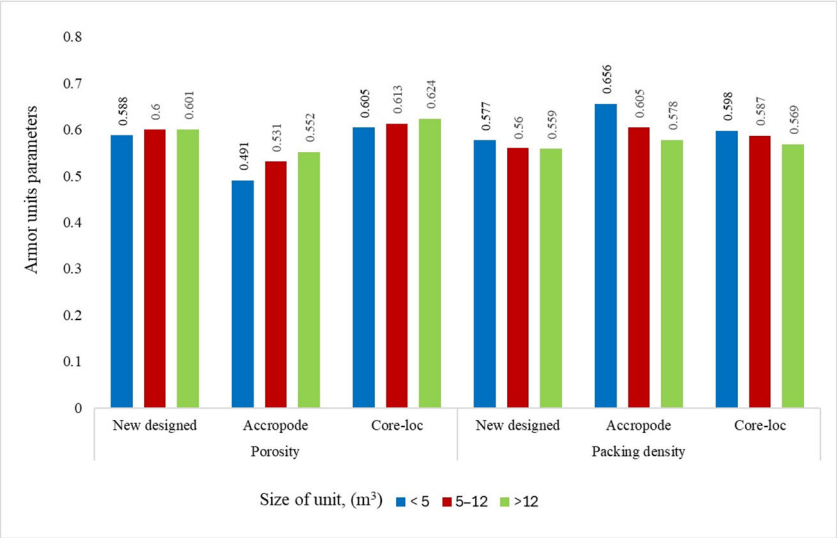

Figure 19. Porosity and packing density of new, accropode, and core-loc armor units at different sizes.

For units smaller in size than 5 m^3, the new design exhibits a porosity of 0.588, which is 16.5% higher than accropode and 2.9% lower than core-loc, while its packing density of 0.577 is 13.7% lower than accropode and 3.6% lower than core-loc. This indicates that, at small scales, the new design creates a more open structure than accropode but avoids the excessive voids of core-loc, suggesting a compromise between hydraulic permeability and structural compactness.

In the medium size range (5–12 m^3), porosity of the new unit (0.600) remains 11.5% higher than accropode but 2.2% lower than core-loc, and its packing density (0.560) is 8.0% lower than accropode and 4.8% lower than core-loc. These results confirm the trend of intermediate performance, showing that the new design can reduce overdensification compared with accropode while still maintaining a tighter packing arrangement than core-loc, which may support improved interlocking and stability.

For large-size units (>12 m^3), the new design has a porosity of 0.601, 8.2% higher than accropode yet 3.8% lower than core-loc, and a packing density of 0.559, which is 3.4% lower than accropode and only 1.8% lower than core-loc. At this scale, the gap in packing density narrows considerably, showing that the new design approaches the hydraulic and structural performance achieved by established units while retaining a balanced void structure.

Overall, the new armor unit consistently positions itself between the two established systems: it is less compact than the accropode but more efficient than the core-loc in terms of hydraulic performance, exhibiting better interlocking and reduced displacement under wave loading. Its porosity values also fall within the upper range without being excessive. This balanced behavior suggests that the new design could deliver improved hydraulic stability and wave energy dissipation while maintaining adequate structural efficiency across all unit sizes.

The double-cube effect (DC) is a practical concept in coastal engineering describing armor units that exhibit hydraulic stability comparable to units with approximately twice their nominal volume. This behavior is generally attributed to enhanced interlocking, multi-directional contact forces, and increased resistance to rotation, which collectively allow a larger portion of the unit's effective mass to participate in wave energy dissipation rather than relying solely on self-weight. Safari I. et al. [30] experimentally demonstrated this mechanism for the double-cube unit, reporting high hydraulic stability ($N_s \approx 2.9$) and efficient overtopping reduction ($\gamma_e \approx 0.46$). Building on this principle, the newly proposed armor unit is geometrically configured to promote similar force redistribution

and interlocking efficiency through a balanced combination of arm extension and central core compactness. This configuration increases porosity relative to accropode—enhancing energy dissipation, while avoiding the excessive void formation observed in core-loc, thereby maintaining competitive packing density and structural continuity. Although a full parametric investigation of individual geometric variables (e.g., arm length and core size) is beyond the scope of the present study, the observed performance trends indicate that the proposed geometry effectively activates the double-cube mechanism, positioning the unit as a scalable and integrated evolution toward simultaneous optimization of hydraulic stability and structural efficiency.

3.2. Stress–Strain Analysis (Structural Integrity)

A stress–strain analysis was performed on the newly designed armor unit. To evaluate the stress response, the unit was subjected to four different loading schemes, as illustrated below. As noted earlier, the unit is made of concrete with a density of 23.56 kN/m^3, a Young's modulus of 21,718,456 kN/m^3, and a Poisson's ratio of 0.17.

3.2.1. First Loading Scheme

The first loading scheme applies a flexural load by placing a 9-ton point load on the center-right side of the unit's upper-right leg, while the upper- and lower-left legs are fixed. Figure 20 presents a three-dimensional view of the unit generated using STAAD.Pro software, illustrating the resulting stress distribution under this loading condition.

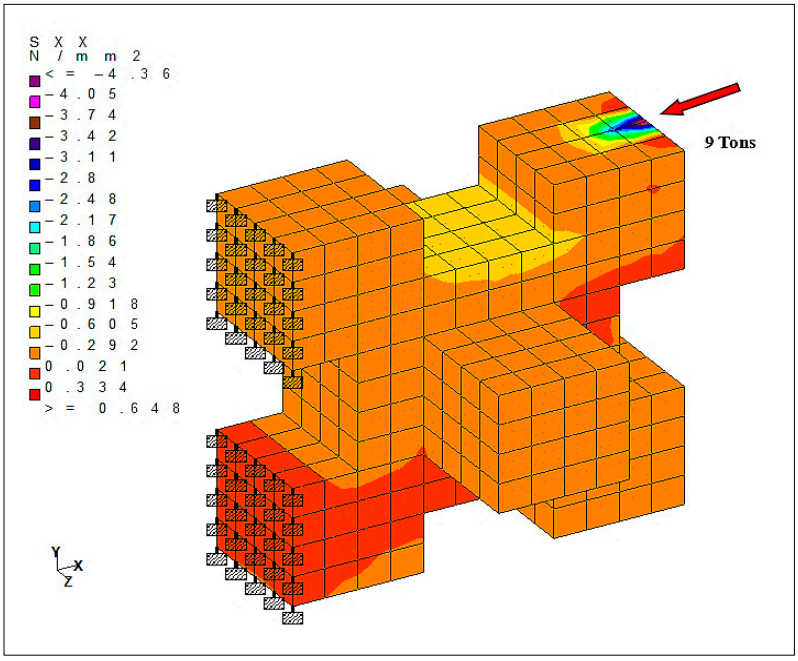

Figure 20. Stresses acting on the unit from the first loading.

3.2.2. Second Loading Scheme

The second loading scheme, also a flexural load, was applied by subjecting a 9-ton point load to the center of the right side of the cube attached to the unit's face, while the upper- and lower-right legs were fixed. Figure 21, generated using STAAD.Pro software, illustrates the unit along with the resulting stress distribution.

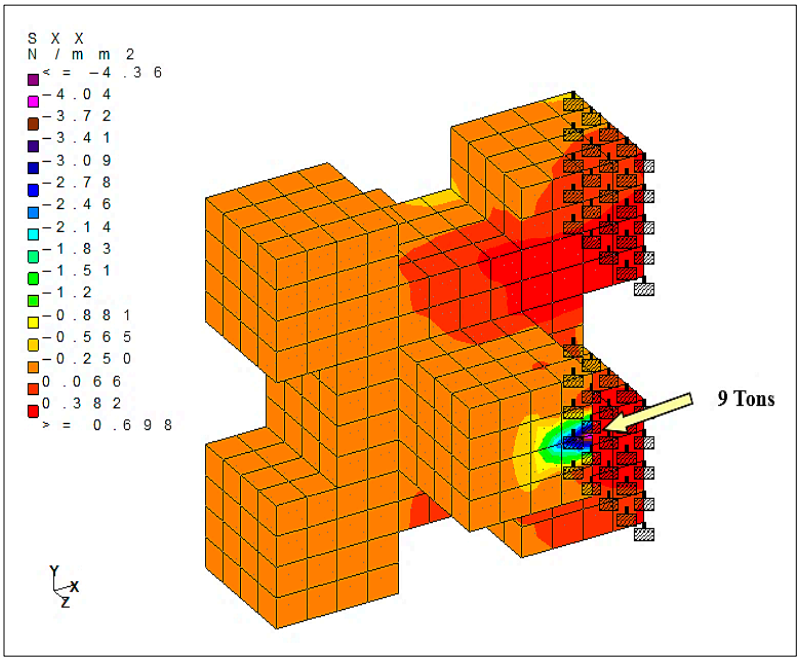

Figure 21. Stresses acting on the unit from second loading.

3.2.3. Third Loading Scheme

The third loading scheme involves torsional loading, applied through four-point loads of 4.5 tons each on the upper and lower legs of the unit. Two of these loads act as pushing forces, while the other two act as pulling forces, creating a twisting effect. The unit is fixed at the central cube attached to its face. The resulting stress distribution is illustrated in Figure 22.

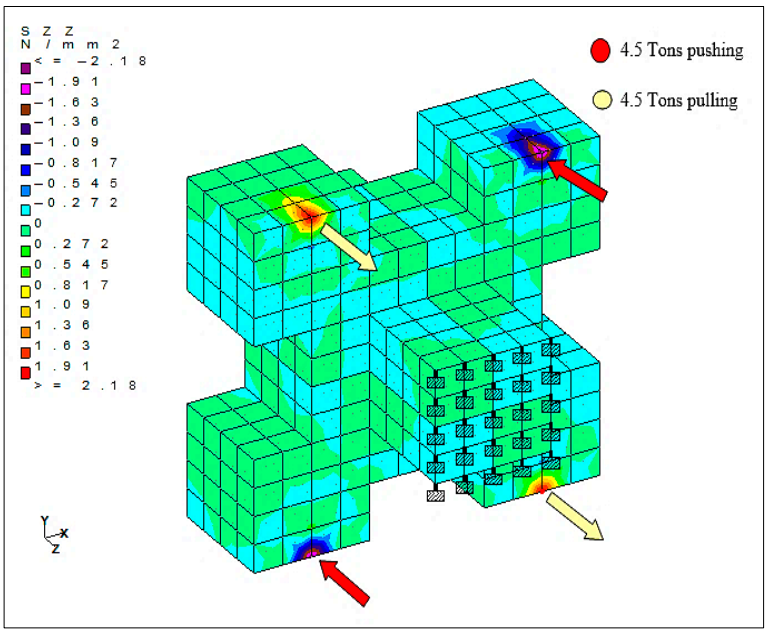

Figure 22. Stresses acting on the unit from the third loading scheme.

3.2.4. Fourth Loading Scheme

The fourth loading scheme is a combination of both flexural and torsional loads. The flexural load is applied as a 9-ton point load acting on the center-right side of the upper-right leg. The torsional load is created by two 4.5-ton loads applied to the face of the upper-

and lower-right legs, with one load pushing and the other pulling. The unit is fixed at both the upper- and lower-left legs. The stresses developed by this combined loading scheme are shown in Figure 23.

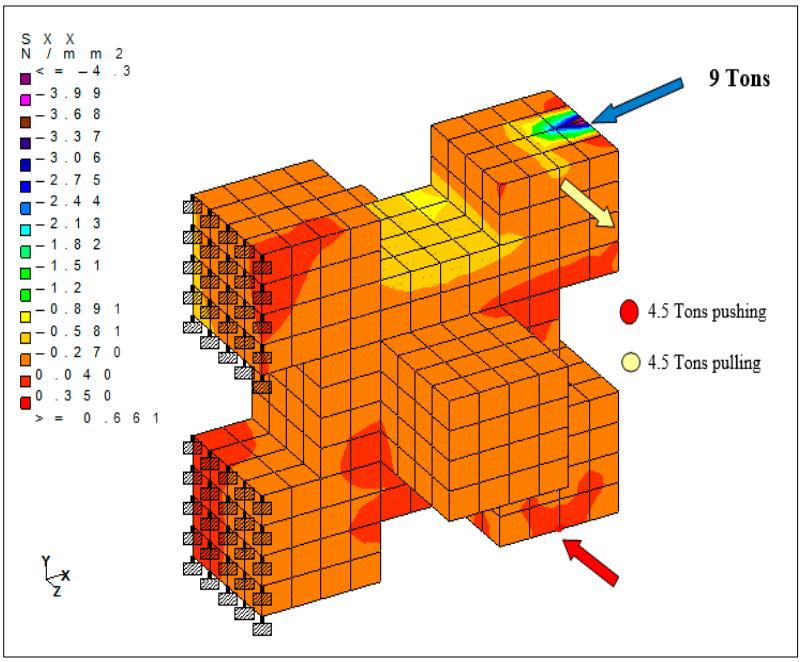

Figure 23. Stresses acting on the unit from the fourth loading scheme.

Maximum tensile stresses were obtained using STAAD.Pro software under four loading schemes: two flexure loadings, torsion, and a combined flexure–torsion case. The software calculated both compression and tensile stresses on the unit for each loading scheme. Table 4 shows the maximum tensile stresses applied to the unit by the four loading schemes.

Table 4. Maximum tensile stresses for four loading schemes.

Type of Loading	Maximum Tensile Stresses
Loading scheme one (flexure)	0.430 MPa
Loading scheme two (flexure)	0.417 MPa
Loading scheme three (torsion)	0.300 MPa
Loading scheme four (torsion and flexure)	0.473 MPa

According to a study conducted by Wurjanto A. and Hardaya A.P. [31] on different types of armor units, the core-loc armor unit exhibited higher tensile stresses than accropode across all loading schemes. Under flexure, core-loc reached about 1.4 MPa, while accropode recorded around 1.2 MPa. For torsion, core-loc again showed a higher value of about 1.5 MPa, compared to 1.0 MPa for accropode. Under the combined flexure and torsion loading, core-loc experienced the highest stress at approximately 2.3 MPa, whereas accropode reached about 1.6 MPa. The newly designed armor unit exhibited lower tensile stresses compared to both the accropode and core-loc.

In particular, the core-loc experienced higher stresses due to its slender sections. This indicates that the new design achieved greater structural integrity, making it equal to or better than existing artificial armor units.

3.3. Hydraulic Stability Evaluation

The hydraulic stability was evaluated using Hudson's formula, where the stability number (H/ΔDn) was plotted against the surf similarity factor (ξ). To enable comparison, two types of armor units were tested: traditional rock and a newly designed unit. The

new armor unit was examined in two different placement configurations, random and uniform. As a result, three types of armor layers were tested: a rock armor layer, a layer with randomly placed new units, and a layer with uniformly placed new units. Tables 5–7 present the results for the three different armor layer configurations. In these tables, the "adjustment number" refers to the position of the rod on the motor's flywheel.

Table 5. Stability results for the rock armor layer.

Adjustment Number	1	2	3	4	5	6	7	8
Wave height (cm)	0.4	1.0	2.0	3.0	4.0	4.3	3.5	2.2
Damage	_	_	start of damage		failure	_	_	_

Table 6. Stability results for the randomly placed newly designed armor unit layer.

Adjustment Number	1	2	3	4	5	6	7	8
Wave height (cm)	0.4	1.0	2.0	3.0	4.0	4.3	3.5	2.2
Damage	_	_	_		rocking	_	_	_

Table 7. Stability results of layer composed of uniformly placed newly designed armor units.

Adjustment Number	1	2	3	4	5	6	7	8
Wave height (cm)	0.4	1.0	2.0	3.0	4.0	4.3	3.5	2.2
Damage	_	_	_	_	_	rocking	_	_

The hydraulic stability behavior of the three armor layers revealed clear differences between the conventional and newly designed systems. Damage progression was recorded visually, in accordance with the approach described by Campos A. et al. [32] and Marino S. et al. [33], where rocking, displacement, and exposure of the underlayer are used as primary indicators of instability in physical model testing.

Figure 24 illustrates the hydraulic stability behavior of the three armor layers, highlighting clear differences between conventional and newly designed systems. Based on visual observations, the rock armor layer showed early weakness, with initial damage occurring at a wave height of 2.0 cm and complete failure at 4.0 cm, corresponding to a stability number of 1.0, where failure was defined as the exposure of the underlayer and core. In contrast, the randomly placed layer of newly designed units withstood higher loading, initiating rocking only at a stability number of approximately 1.4, while the uniformly placed layer of newly designed units performed even better, with rocking observed at 1.5 and no failure recorded throughout the test sequence. These results demonstrate that, unlike traditional rock armor, which is prone to early instability, the newly designed units combine enhanced hydraulic energy dissipation with structural compactness, resulting in improved resilience under wave attack. The present flume program is intentionally positioned as a comparative hydraulic assessment, aimed at identifying rocking, sliding, and displacement thresholds under controlled and repeatable wave conditions prior to broader physical testing. Within this framework, the new units exhibited significantly higher stability margins than conventional rock armor, with rock failure occurring at Ns = 1.0, whereas the newly designed units initiated rocking at Ns = 1.4–1.5, without progressing to failure. Consequently, the proposed design effectively overcomes the early failure limitations of rock armor and represents a meaningful step toward more stable and scalable solutions for breakwater protection.

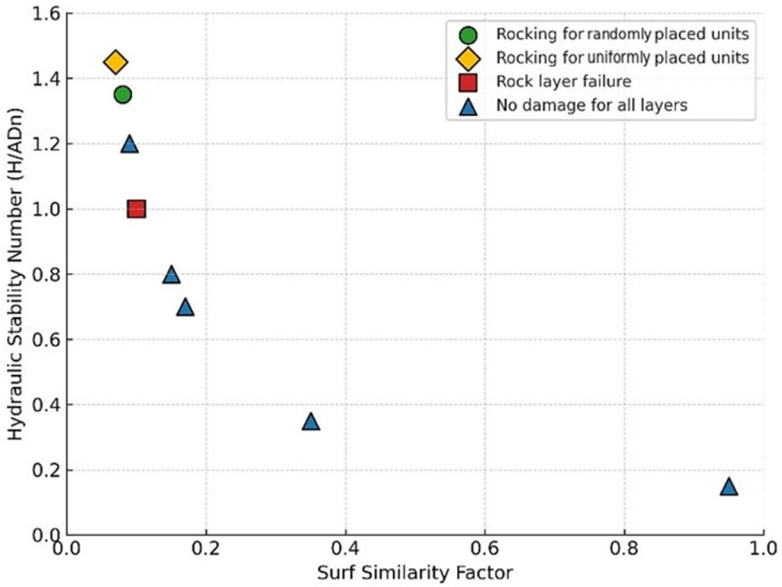

Figure 24. Hydraulic stability for the three armor layers.

Two notable phenomena were observed during the hydraulic stability testing. First, at the highest rod adjustment, incident waves were observed to break prior to reaching the structure's cross-section. This early breaking reduced the wave height and, consequently, the wave energy exerted on the structure. Therefore, adjustments had to be made to ensure that wave breaking would not occur prior to the structure's position. Second, for the randomly placed concrete armor units, the onset of rocking did not lead to progressive damage. Instead, the units exhibited a self-stabilizing response, gradually migrating downslope and interlocking with adjacent units. This automatic interlocking mechanism contributed to improved structural stability under wave action.

Nielsen A.F. and Gordon A.D. [34] investigated the stability of revetment rock armor under depth-limited breaking waves and introduced an energy-based predictive formula to replace traditional Hudson-type methods. Their results showed that rock armor becomes unstable at relatively low thresholds of wave loading, with stability numbers close to 1.0 leading to damage or failure depending on depth and slope conditions. By comparison, our findings show that while rock armor fails at $N_s \approx 1.0$, the newly designed units withstand much higher loads, initiating rocking only at 1.4 (random placement) and 1.5 (uniform placement) without failure.

This represents a 40–50% improvement in stability number over conventional rock armor. Therefore, while Nielsen and Gordon advanced predictive modeling of rock stability under shallow-water wave energy, our results go further by demonstrating experimentally that engineered units not only surpass rock in hydraulic stability but also extend the design framework to placement-sensitive and practical solutions.

3.4. Run-Up Test Results

Run-up testing was performed using the same cross-section applied in the hydraulic stability experiments. The procedure involved measuring the maximum vertical distance reached by waves impacting the slope. The test was conducted under the same wave height and water depth conditions as those used in the hydraulic stability assessment. Furthermore, the same three armor layers examined in the hydraulic stability test were employed in this evaluation. The run-up results for each layer are presented below in Tables 8–10.

Table 8. Run-up test results for rock armor layer.

Wave Height (cm)	0.4	1.0	2.0	3.0	4.0	4.3	3.5	2.2
R (cm)	2.5	3.3	4.1	6.0	6.7	7.0	6.3	4.0

Table 9. Run-up test results for randomly placed armor units.

Wave Height (cm)	0.4	1.0	2.0	3.0	4.0	4.3	3.5	2.2
R (cm)	1.2	2.9	3.8	4.6	4.8	5.5	5.0	3.8

Table 10. Run-up test results for uniformly placed units.

Wave Height (cm)	0.4	1.0	2.0	3.0	4.0	4.3	3.5	2.2
R (cm)	1.7	3.1	4.0	5.0	5.3	6.5	5.4	4.0

Figure 25 presents the run-up test results, which show that the newly designed armor units consistently reduce run-up compared to rock armor, with the scale of reduction varying by wave height. At low wave heights (0.4–1.0 cm), reductions were substantial, with random placement lowering run-up by about 50% and uniform placement by around 30%, indicating strong energy dissipation at small wave loads. At moderate wave heights (2.0–2.2 cm), the differences narrowed to about 5–12%, showing performance convergence with rock armor.

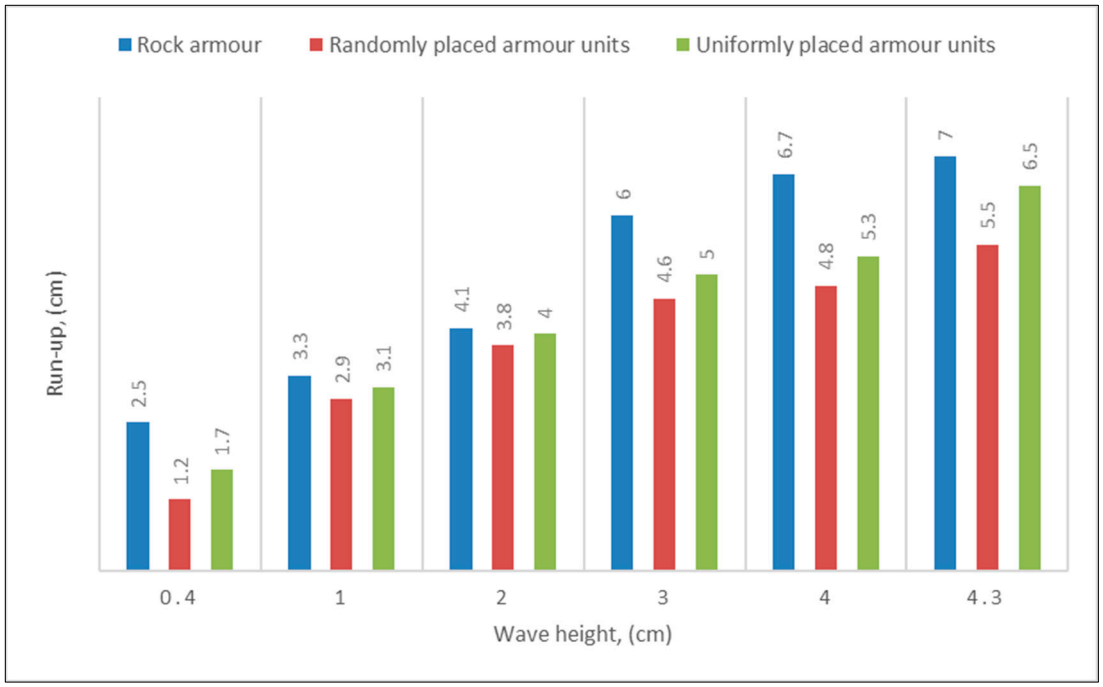

Figure 25. Run-up results for the three armor layers.

At intermediate wave heights (3.0–3.5 cm), the advantages increased again, with random placement achieving 21–23% lower run-up and uniform placement 14–17% lower than rock armor. Finally, at high wave heights (4.0–4.3 cm), reductions peaked once more, with random placement cutting run-up by 21–28% and uniform placement by 7–21%. Overall, the findings demonstrate that the new design consistently enhances hydraulic efficiency, with random placement producing greater reductions at extreme wave heights, while uniform placement delivers more reliable improvements across all conditions.

Buccino M. et al. [35] investigated Ecopode units (single-layer concrete armor with a rock-like skin) under spectral/random wave conditions and showed that their rough surface enhanced energy dissipation, leading to moderate reductions in run-up compared to conventional rock slopes, particularly for steeper slopes and energetic waves. However, when compared with our findings, the newly designed armor units demonstrate superior performance across stages. At low wave heights, reductions were much greater (50% for random placement and 30% for uniform), while moderate wave heights showed smaller decreases (5–12%), similar to Ecopode's narrowing effect. At high wave heights, our units again outperformed, reducing run-up by (20–30%), exceeding the values reported for Ecopode. In summary, while Buccino M. et al. confirmed the benefit of roughened concrete armor, our results demonstrate larger and more consistent run-up reductions across the full wave range, representing a step forward beyond their findings.

3.5. Overtopping Behavior

For the overtopping test, it was essential to ensure that overtopping occurred; therefore, the water depth was increased to 20 cm. A single wave height was employed, corresponding to the maximum generated by the wave generator (4.3 cm). The objective of this test was to quantify the volume of overtopping on the slope. This was achieved by measuring the amount of water collected in the basin. The same three armor layers described earlier in this chapter were also used in this test. The results for the three layers are given below in Table 11.

Table 11. Overtopping results for the three armor layers.

Type of Armor Layer	Amount of Overtopping by (cm^3)
Rock armor layer	1500
Randomly placed units	620
Uniformly placed units	940

The overtopping results in Table 11 clearly highlight the superior performance of the new design. The randomly placed newly designed armor units transmitted only 620 cm^3, the lowest among all configurations. In comparison, the rock armor layer allowed 1500 cm^3, which is about 142% higher, while the uniformly placed newly designed armor units transmitted 940 cm^3, approximately 52% higher. These results confirm that the randomly placed newly designed units achieved the most effective resistance to overtopping, while the uniformly placed newly designed units also performed considerably better than conventional rock armor but remained less effective than the random arrangement.

Bruce T. et al. [36] reported that advanced single-layer units such as accropode and core-loc achieved overtopping reductions of about 35–45% compared with rock armor, while Xbloc performed slightly better with reductions of up to 50%, and simpler units like cubes and tetrapods showed smaller decreases of only 15–25%. In comparison, our study demonstrated overtopping reductions of approximately 37% for uniformly placed newly designed units and nearly 59% for randomly placed units. This indicates that the uniform placement of our design performs on par with the best results from Bruce T. et al., while the random placement clearly surpasses them, establishing superior resistance to transmitted overtopping and advancing beyond the performance achieved in earlier studies

4. Conclusions

In this study, a newly designed artificial armor unit was developed and assessed for its potential application in the armor layers of offshore rubble mound breakwaters. The performance of the proposed unit was examined through comparative analyses against conventional armor units, considering key parameters such as hydraulic stability, wave

run-up, overtopping, economic efficiency, armor layer porosity, and ease of placement. The concluding section provides a synthesis of the obtained results, presents the main conclusions, and outlines recommendations to guide future research and practical applications. The conclusions drawn from this study are listed below:

1. The geometric efficiency of the newly designed armor unit in comparison to the accropode and core-loc designs demonstrates a superior balance between compactness and permeability. When it comes to porosity, the new armor unit achieved a porosity 8–16% higher than that of accropode, hence achieving better energy dissipation. However, the new unit achieved a lower porosity (2–4%) than that of core-loc, but it remains a more robust structural matrix. Furthermore, the newly designed unit reduced packing density by 2–14% in comparison to both accropode and core-loc, indicating a more efficient utilization of material, offering a cost-efficient alternative in which it optimizes concrete volume per unit area of protection.
2. Mechanical analysis reveals that the geometric configuration of the newly designed armor unit mitigates stress concentrations more effectively. Under loading schemes that include flexure, torsion, and combined loading, the new unit exhibited a 8–15% reduction in internal stress when compared to accropode. In addition, a reduction in stress concentrations reaching 20–35% in comparison to core-loc was observed. These results hint that the double-cube geometry succeeded in redistributing loads, providing a more robust structural alternative that minimizes breakage of the armor unit.
3. When compared to traditional rock armor units, the newly designed unit provides superior stability and reduces wave–structure interaction. The proposed unit remained stable at higher loading, with rocking only initiated at Ns equal to 1.4 when randomly placed and at 1.5 when uniformly placed, while rock armor units reached failure at an Ns reading of 1.0. Randomly placed units achieved a 50% reduction in run-up during peak conditions, while uniform placed units achieved a 30% reduction. Furthermore, the proposed unit was effective in preventing overtopping. Randomly placed armor units reduced overtopping by approximately 59% in comparison to rock armor units, while uniformly placed units reduced the overtopping by 37%, confirming the design's efficient protection of the leeward infrastructure.

The newly designed armor unit showed superior structural integrity, interlocking, and hydraulic stability, while being more economical and efficient than conventional rock armor and existing units. This study is limited by the absence of tests on wave reflection, transmission, and large-scale hydraulic performance of the newly designed armor unit. Future work should therefore include flume studies at larger scales, field applications on existing breakwaters, and full-scale drop tests to assess structural resilience. In addition, developing practical formwork and evaluating casting efficiency are recommended to validate constructability and economic feasibility

Author Contributions: Conceptualization, M.Z.A.-M.; Methodology, M.Z.A.-M.; Formal analysis, M.Z.A.-M. and M.K.I.; Investigation, A.K.; Resources, Z.H.O., A.K. and Z.E.; Writing—original draft, S.S.H., H.F., L.F.W. and T.M.H.; Writing—review & editing, S.S.H., H.F., L.F.W. and T.M.H.; Supervision, M.S.N. and A.S.; Project administration, T.M.H., M.S.N. and A.S. All authors have read and agreed to the published version of the manuscript.

Funding: This research received no external funding.

Institutional Review Board Statement: Not applicable.

Informed Consent Statement: Not applicable.

Data Availability Statement: The original contributions presented in this study are included in the article. Further inquiries can be directed to the corresponding author.

Conflicts of Interest: The authors declare no conflicts of interest.

References

1. Ismail Ahmed Ahmed Meligy, S. The artistic development of the sea element in ancient civilizations. *Int. J. Multidiscip. Stud. Art Technol.* **2021**, *4*, 74–101. [CrossRef]
2. Costello, C.; Cao, L.; Gelcich, S.; Cisneros-Mata, M.Á.; Free, C.M.; Froehlich, H.E.; Golden, C.D.; Ishimura, G.; Maier, J.; Macadam-Somer, I.; et al. The future of food from the sea. *Nature* **2020**, *588*, 95–100. [CrossRef] [PubMed]
3. Alves, B.; Angnuureng, D.B.; Morand, P.; Almar, R. A review on coastal erosion and flooding risks and best management practices in West Africa: What has been done and should be done. *J. Coast. Conserv.* **2020**, *24*, 38. [CrossRef]
4. Kindeberg, T.; Almström, B.; Skoog, M.; Olsson, P.A.; Hollander, J. Toward a multifunctional nature-based coastal defense: A review of the interaction between beach nourishment and ecological restoration. *Nord. J. Bot.* **2023**, *2023*, e03751. [CrossRef]
5. Morris, R.L.; Heery, E.C.; Loke, L.H.; Lau, E.; Strain, E.; Airoldi, L.; Alexander, K.A.; Bishop, M.J.; Coleman, R.A.; Cordell, J.R.; et al. Design options, implementation issues and evaluating success of ecologically engineered shorelines. In *Oceanography and Marine Biology*; CRC Press: Boca Raton, FL, USA, 2019.
6. Whitesell, L.A. Seismic reflection and beach nourishment–lessons from Hurricane Sandy. In Proceedings of the SEG International Exposition and Annual Meeting, Houston, TX, USA, 22–27 September 2013; p. SEG-2013-1494.
7. Iskander, M.M.; Frihy, O.E.; El Ansary, A.E.; Abd El Mooty, M.M.; Nagy, H.M. Beach impacts of shore-parallel breakwaters backing offshore submerged ridges, Western Mediterranean Coast of Egypt. *J. Environ. Manag.* **2007**, *85*, 1109–1119. [CrossRef]
8. Himi, T.H. Experimental Study on the Performance of Multilayer Geotube Breakwater with and without CC Block under Wave Attack. Master's Thesis, Bangladesh University of Engineering and Technology, Dhaka, Bangladesh, 2022.
9. Rahmstorf, S. Rising hazard of storm-surge flooding. *Proc. Natl. Acad. Sci. USA* **2017**, *114*, 11806–11808. [CrossRef]
10. Apu, N.; Das, U. Tectonics and earthquake potential of Bangladesh: A review. *Int. J. Disaster Resil. Built Environ.* **2021**, *12*, 295–307. [CrossRef]
11. Pires, A.; Chaminé, H.I.; Piqueiro, F.; Rocha, F. Coastal geo-engineering techniques for the assessment of rock armour structures. *Mar. Georesour. Geotechnol.* **2014**, *32*, 155–178. [CrossRef]
12. Jiao, L.; Liu, C.; Jiang, D.; Zhang, X.; Lv, X. Storm surge numerical simulation of Typhoon "Mangkhut" with adjoint data assimilation. *J. Mar. Sci. Eng.* **2025**, *13*, 1992. [CrossRef]
13. Gökdağ, A. Assessment of Storm Damaged Breakwater and Reinforced Cross-Section. Master's Thesis, Middle East Technical University, Ankara, Türkiye, 2025.
14. Suwondo, R.; Keintjem, M.; Suangga, M.; Altaee, M. The Influence of the Armor Stability Coefficient on the Hydraulic, Economic, and Environmental Performance of Rubble Mound Breakwaters. *Eng. Technol. Appl. Sci. Res.* **2025**, *15*, 28475–28480. [CrossRef]
15. van Gent, M.R.; Wolters, G.; Capel, A. Wave overtopping discharges at rubble mound breakwaters including effects of a crest wall and a berm. *Coast. Eng.* **2022**, *176*, 104151. [CrossRef]
16. Hudson, R.Y. Laboratory investigation of rubble-mound breakwaters. *J. Waterw. Harb. Div.* **1959**, *85*, 93–121. [CrossRef]
17. Van der Meer, J.W.; Pilarczyk, K.W. Stability of rubble mound breakwaters under random wave attack. In Proceedings of the 19th International Conference on Coastal Engineering, Houston, TX, USA, 3–7 September 1984.
18. Sayar, S.D.; Baker, S.; Nistor, I.; Martinez, J.G. Hydraulic performance of ecofriendly breakwater armour units. In Proceedings of the 38th Conference on Coastal Engineering, Rome, Italy, 8–14 September 2024; Volume 38, ISBN 978-0-9896611-7-1. [CrossRef]
19. Safa, E.; Mojtahedi, A.; Mohammadian, A.; Yaghin, M.A. Hydrodynamic assessment of a new nature-based armour unit on rubble mound breakwater for coastal protection. *China Ocean Eng.* **2024**, *38*, 439–452. [CrossRef]
20. Park, Y.H.; Oh, Y.M.; Ahn, S.M.; Han, T.H.; Kim, Y.T.; Suh, K.D.; Won, D. Development of a new concrete armor unit for high waves. *J. Coast. Res.* **2019**, *35*, 719–728. [CrossRef]
21. Leone, E.; Francone, A.; Paglialunga, A.; Ciardulli, F.; Long, J.; Aloisi, A.; Tomasicchio, G.R. Overtopping Assessment of a Rubble Mound Breakwater with Innovative Armor Units: A Physical and Numerical Study. *J. Coast. Res.* **2025**, *113*, 804–808. [CrossRef]
22. Mousavi, S.H.; Kavianpour, M.R.; Aminoroayaie Yamini, O. Experimental analysis of breakwater stability with antifer concrete block. *Mar. Georesour. Geotechnol.* **2017**, *35*, 426–434. [CrossRef]
23. Khodadoust, H. Evaluation of armoured breakwater alternatives using a multi-criteria approach: Case study of a fishery port in Southern Iran. *Reg. Stud. Mar. Sci.* **2025**, *91*, 104566. [CrossRef]
24. Oumeraci, H.; Recio, J. Geotextile sand containers for shore protection. In *Handbook of Coastal and Ocean Engineering*; World Scientific Publishing Company: Singapore, 2018; pp. 775–822.
25. Aliasgary, S.; Badiei, S.P.; Mouazé, D. Evaluation of the Factors Affecting the Hydraulic Stability of Tblock™ Coastal Protection Armour Unit. *Water Waves* **2024**, *6*, 571–592. [CrossRef]

26. van der Meer, J.; van Gent, M.; Wolters, G.; Heineke, D. New Design Guidance for Underlayers and Filter Layers for Rock Armour under Wave Attack. In *Coasts, Marine Structures and Breakwaters 2017: Realising the Potential*; ICE Publishing: London, UK, 2018; pp. 1069–1079.
27. Etemad-Shahidi, A.; Bali, M.; Van Gent, M.R. On the stability of rock armored rubble mound structures. *Coast. Eng.* **2020**, *158*, 103655. [CrossRef]
28. Gao, Z.; Wang, Z.; Chen, Y.; Li, S.; Li, L.; Chen, L.; Huang, C.; Yang, Q. Study on the damage effect of 12.7 mm armour piercing incendiary projectile penetrating aramid reinforced concrete slab. *Comput. Struct.* **2025**, *312*, 107706. [CrossRef]
29. Özvan, A.; Dinçer, İ.; Acar, A. Quality assessment of geo-materials for coastal structures (Yumurtalık, Turkey). *Mar. Georesour. Geotechnol.* **2011**, *29*, 299–316. [CrossRef]
30. Safari, I.; Mouazé, D.; Aliasgary, S.; Carpentier, G.; Ropert, F. Hydraulic response and overtopping performance of single-layer double cube unit armored mound breakwater. *J. Mar. Sci. Eng.* **2023**, *11*, 1382. [CrossRef]
31. Wurjanto, A.; Hardaya, A.P. Quantitative consideration in selection of breakwater concrete armor unit based on unit's internal tensile stress response. *IOP Conf. Ser. Earth Environ. Sci.* **2022**, *1065*, 012021. [CrossRef]
32. Campos, Á.; Castillo, C.; Molina-Sanchez, R. Damage in rubble mound breakwaters. Part I: Historical review of damage models. *J. Mar. Sci. Eng.* **2020**, *8*, 317. [CrossRef]
33. Marino, S.; Galantucci, R.A.; Saponieri, A. Measuring rock slope damage on rubble mound breakwater through digital photogrammetry. *Measurement* **2023**, *211*, 112656. [CrossRef]
34. Nielsen, A.F.; Gordon, A.D. Revetment Rock Armour Stability Under Depth-Limited Breaking Waves. *Coasts* **2025**, *5*, 12. [CrossRef]
35. Buccino, M.; Calabrese, M.; Ciardulli, F.; Di Pace, P.; Tomasicchio, G.R. One layer concrete armor units with a rock-like skin: Wave reflection and run-up. *J. Coast. Res.* **2011**, *SI 64*, 469–473.
36. Bruce, T.; Van der Meer, J.W.; Franco, L.; Pearson, J.M. Overtopping performance of different armour units for rubble mound breakwaters. *Coast. Eng.* **2009**, *56*, 166–179. [CrossRef]